Internet of Things Meets Brain–Computer Interface: A Unified Deep Learning Framework for Enabling Human-Thing Cognitive Interactivity

Xiang Zhang, *Graduate Student Member, IEEE*, Lina Yao, *Member, IEEE*, Shuai Zhang, *Student Member, IEEE*, Salil Kanhere, *Senior Member, IEEE*, Michael Sheng, *Member, IEEE*, and Yunhao Liu, *Fellow, IEEE*

***Abstract*—A brain–computer interface (BCI) acquires brain signals, analyzes, and translates them into commands that are relayed to actuation devices for carrying out desired actions. With the widespread connectivity of everyday devices realized by the advent of the Internet of Things (IoT), BCI can empower individuals to directly control objects such as smart home appliances or assistive robots, directly via their thoughts. However, realization of this vision is faced with a number of challenges, most importantly being the issue of accurately interpreting the intent of the individual from the raw brain signals that are often of low fidelity and subject to noise. Moreover, preprocessing brain signals and the subsequent feature engineering are both time-consuming and highly reliant on human domain expertise. To address the aforementioned issues, in this paper, we propose a unified deep learning-based framework that enables effective human-thing cognitive interactivity in order to bridge individuals and IoT objects. We design a reinforcement learning-based selective attention mechanism (SAM) to discover the distinctive features from the input brain signals. In addition, we propose a modified long short-term memory to distinguish the interdimensional information forwarded from the SAM. To evaluate the efficiency of the proposed framework, we conduct extensive real-world experiments and demonstrate that our model outperforms a number of competitive state-of-the-art baselines. Two practical real-time human-thing cognitive interaction applications are presented to validate the feasibility of our approach.**

***Index Terms*—Brain–computer interface (BCI), cognitive, deep learning (DL), Internet of Things (IoT).**

I. Introduction

IT IS expected that by 2020 over 50 billion devices will be connected to the Internet. The proliferation of the Internet of Things (IoT) is expected to improve efficiency and impact various domains including home automation, manufacturing and industries, transportation, and healthcare [1]. Individuals will have the opportunity to interact and control a wide range of everyday objects through various means of interactions including applications running on their smartphone or wearable devices, voice, and gestures. brain–computer interface (BCI)[1] is emerging as a novel alternative for supporting interaction between IoT objects and individuals. BCI establishes a direct communication pathway between human brain and an external device thus eliminating the need for typical information delivery methods [2]. Recent trends in BCI research have witnessed the translation of human thinking capabilities into physical actions, such as mind-controlled wheelchairs and IoT-enabled appliances [3], [4]. These examples suggest that the BCI is going to be a major aiding technology in human-thing interaction [5].

BCI-based cognitive interactivity offers several advantages. One is the inherent privacy arising from the fact that brain activity is invisible and thus impossible to observe and replicate [6]. The other is the convenience and real-time nature of the interaction, since the human only needs to think of the interaction rather than undertake the corresponding physical motions (e.g., speak, type, and gesture) [7].

However, the BCI-based human-thing cognitive interactivity faces several challenges. While the brain signals can be measured using a number of technologies such as electroencephalogram (EEG) [2], functional near-infrared spectroscopy (fNIR) [8], and magnetoencephalography (MEG) [9], all of these methods are susceptible to low fidelity and are also easily influenced by environmental factors and sentiment status (e.g., noise and concentration) [10]. In other words, the brain signals generally have very low signal-to-noise ratios, and inherently lack sufficient spatial or temporal resolution and insight on activities of deep brain structures [5]. As a result, while current cognitive recognition systems can achieve about 70%–80% accuracy, this is not sufficient to design practical systems. Second, data preprocessing, parameter selection (e.g., filter type, filtering band, segment window, and overlapping), and feature engineering (e.g., feature selection and extraction both in the time domain and frequency domain) are all time-consuming and highly dependent on human expertise in the domain [11].

Manuscript received May 11, 2018; revised July 31, 2018; accepted October 20, 2018. Date of publication October 24, 2018; date of current version May 8, 2019. *(Corresponding author: Xiang Zhang.)*

X. Zhang, L. Yao, S. Zhang, and S. Kanhere are with the School of Computer Science and Engineering, University of New South Wales, Kensington, NSW 2052, Australia (e-mail: xiang.zhang3@student.unsw.edu.au; lina.yao@unsw.edu.au; shuai.zhang@student.unsw.edu.au; salil.kanhere@unsw.edu.au).

M. Sheng is with the Department of Computing, Macquarie University, Sydney, NSW 2109, Australia (e-mail: michael.sheng@mq.edu.au).

Y. Liu is with the Department of Computer Science and Engineering, Michigan State University, East Lansing, MI 48824 USA (e-mail: yunhao@cse.msu.edu).

Digital Object Identifier 10.1109/JIOT.2018.2877786

[1]The BCI mentioned in this paper refers to noninvasive BCI.

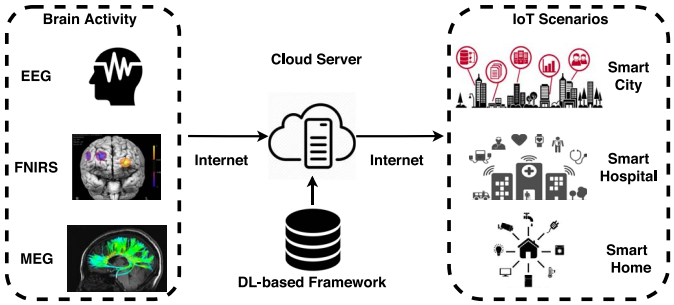

Fig. 1. Schematic of cognitive IoT framework.

To address the aforementioned issues, in this paper, we propose a unified deep learning (DL) [12] framework for enabling human-thing cognitive interactivity. As shown in Fig. 1, our framework measures the user's brain activity (such as EEG, FNIRS, and MEG) through a specific brain signal collection equipment. The raw brain signals are forwarded to the cloud server via Internet access. The cloud server uses a person-dependent pretrained DL model for analyzing the raw signals. The analysis results interpreted signals could be used for actuating functions in a wide range of IoT applicants, such as smart city [13] (e.g., transportation control and agenda schedule), smart hospital [14], [15] (e.g., emergency call and anomaly mentoring), and smart home [16], [17] (e.g., appliances control and assistive robot control).

The proposed unified DL framework aims to interpret the subjects' intent and decode it into the corresponding commands which are discernible for the IoT devices. Based on our previous study [5], [18], for each single brain signal sample, the self-similarity is always higher than the cross-similarity, which means that the intraintent cohesion of the samples is stronger than the interintent cohesion. In this paper, we propose a weighted average spatial long short-term memory (WAS-LSTM) to exploit the latent correlation between signal dimensions. The proposed end-to-end framework is capable of modeling high-level, robust, and salient feature representations hidden in the raw human brain signal streams and capturing complex relationships within data. The main contributions of this paper are highlighted as follows.

1) We propose a unified DL-based framework to interpret individuals' brain activity for enabling human-thing cognitive interactivity. To our best knowledge, we are the very first work that bridging BCI and IoT to investigate end-to-end cognitive brain-to-thing interaction.
2) We apply deep reinforcement learning, with designed reward, state, and action model, to automatically discover the most distinguishable features from the input brain signals. The discovered features are forwarded to a modified DL structure, in particular, the proposed WAS-LSTM, to capture the cross-dimensional dependency in order to recognize user's intention.
3) We also present two operational prototypes of the proposed framework: a brain typing system and a cognitive controlled smart home service robot, which demonstrate the efficacy and practicality of our approach.

II. Proposed Framework

In this section, we present the cognition detection framework in detail. The subjects' brain activity can be measured by a number of methods like EEG, fMRI, and MEG. In this paper, we exploit EEG due to its unique features, such as low-cost, low-energy, privacy, and portability. The proposed framework is depicted in Fig. 2. The main focus of the approach is to exploit the latent dependency among different signal dimensions. To this end, the proposed framework contains several components: 1) the replicate and shuffle (RS) processing; 2) the selective attention learning; and 3) the sequential LSTM-based classification. In the following, we will first discuss the motivations of the proposed method and then introduce the aforementioned components in details.

A. Motivation

How to exploit the latent relationship between EEG signal dimensions is the main focus of the proposed approach. The signals belonging to different cognitions are supposed to have different interdimension dependent relationships which contain rich and discriminative information. This information is critical to improve the distinctive signal pattern discovery.

In practice, the EEG signal is often arranged as 1-D vector, the signal is less informative for the limited and fixed element arrangement. The elements order and the number of elements in each signal vector can affect the element dependency. For example, the interdimension dependency in $\{0, 1, 2, 3, 4\}$ and $\{1, 2, 3, 4, 0\}$ are not reciprocal; similarly, $\{0, 1, 2, 3, 4\}$ and $\{0, 1, 1, 2, 3, 4\}$ are not reciprocal. In many real-world scenarios, the EEG data are concatenated following the distribution of biomedical EEG channels. Unfortunately, the practical channel sequence, with the fixed order and number, may not be suitable for interdimension dependency analysis. Therefore, we propose the following three techniques to amend the drawback.

First, we RS the input EEG signal vector on dimension-wise in order to provide as much latent dependency as possible among feature dimensions (Section II-B).

Second, we introduce a focal zone as a selective attention mechanism (SAM), where the optimal interdimension dependency for each sample only depends on a small subset of features. Here, the focal zone is optimized by deep reinforcement learning which has been shown to achieve both good performance and stability in policy learning (Section II-C).

Third, we propose the WAS-LSTM classifier by extracting the distinctive interdimension dependency (Section II-D).

B. Data Replicate and Shuffle

Suppose the input EEG data can be denoted by $\mathbf{X} = \{(\mathbf{x}_i, y_i), i = 1, 2, \ldots, I\}$ where $(\mathbf{x}_i, y_i)$ denotes the 1-D EEG signal, called one *sample* in this paper, and I denotes the number of samples. In each sample, the feature $\mathbf{x}_i \in \mathbb{R}^K$ contains K elements and the corresponding ground truth $y_i \in \mathbb{R}$ is an integer that denotes the sample's category. Different categories correspond to various brain activities. $\mathbf{x}_i$ can be described as a vector with K elements, $\mathbf{x}_i = \{x_{ik}, k = 1, 2, \ldots, K\}$.

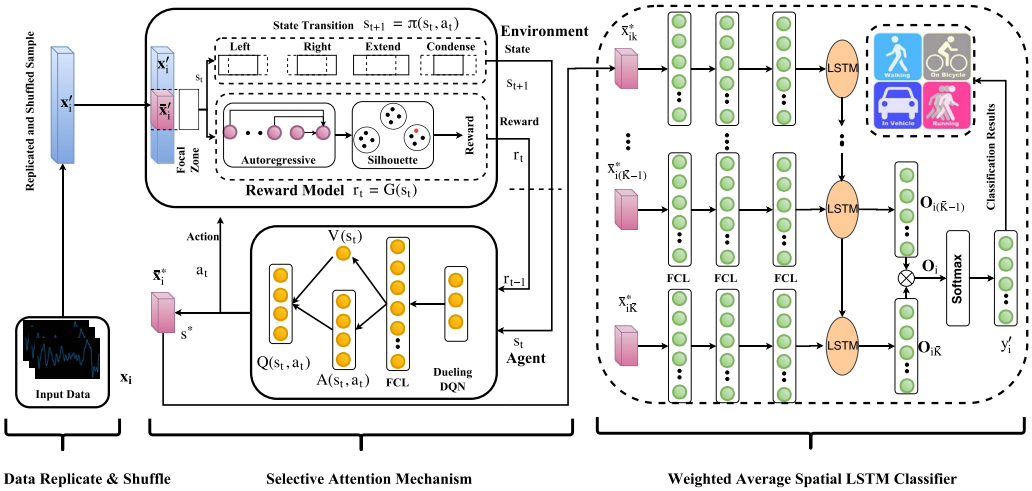

Fig. 2. Flowchart of the proposed framework. The focal zone $\bar{\mathbf{x}}_i$ is a selected fragment from $\mathbf{x}'_i$ to feed in the state transition and the reward model. In each step t, one action is selected by the state transition to update s_t based on the agent's feedback. The reward model evaluates the quality of the focal zone to the reward r_t. The dueling DQN is employed to find the optimal focal zone $\bar{\mathbf{x}}^*_i$ which will be feed into the LSTM-based classifier to explore the interdimension dependency and predict the sample's label y'_i. FCL denotes fully connected layer. The state transition contains four actions: left shifting, right shifting, extend, and condense. The dashed line indicates the focal zone before the action while the solid line indicates the position of the focal zone after the action.

To provide more potential interdimension spatial dependencies, we propose a method called RS. RS is a two-step feature transformation method which maps $\mathbf{x}_i$ to a higher dimensional space $\mathbf{x}'_i$ with more complete element combinations

$$\mathbf{x}_i \in \mathbb{R}^K \rightarrow \mathbf{x}'_i \in \mathbb{R}^{K'}, \ K' > K.$$

In the first step (replicate), we replicate $\mathbf{x}_i$ for $h = K'\%K + 1$ times where $\%$ denotes remainder operation. Then we get a new vector with length as $h * K$ which is not less than K'; in the second step (shuffle), we randomly shuffle the replicated vector in the first step and intercept the first K' element to generate $\mathbf{x}'_i$. Theoretically, compared to $\mathbf{x}_i$, the number and order of elements in $\mathbf{x}'_i$ are more diverse. For instance, set $\mathbf{x}_i = \{1, 3, 4, 2\}$, in which the four elements are arranged in a fixed order and limited combinations, it is difficult to mine the latent pattern in $\mathbf{x}_i$; however, set the replicated and shuffled signal as $\mathbf{x}'_i = \{3, 1, 2, 3, 4, 4, 1, 2\}$, the equal difference characteristic is easy to be found in the fragment $\{1, 2, 3, 4\}$ (the second to fifth elements of $\mathbf{x}'_i$). Therefore, a major challenge in this paper is to discover the fragment with rich distinguishable information. To solve this problem, we propose a attention-based selective mechanism which is detailed introduced in Section II-C.

C. Selective Attention Mechanism

In the next process, we attempt to find the optimal dependency which includes the most distinctive information. But K', the length of $\mathbf{x}'_i$, is too large and is computationally expensive. To balance the length and the information content, we introduce the *attention mechanism* [19] to emphasize the informative fragment in $\mathbf{x}'_i$ and denote the fragment by $\bar{\mathbf{x}}_i$, which is called *focal zone*. Suppose $\bar{\mathbf{x}}_i \in \mathbb{R}^{\bar{K}}$ and $\bar{K}$ denotes the length of the focal zone. For simplicity, we continue to denote the kth element by $\bar{\mathbf{x}}_{ik}$ in the focal zone. To optimize the focal zone, we employ deep reinforcement learning as the optimization framework for its excellent performance in policy optimization [20].

1) Overview: As shown in Fig. 2, the focal zone optimization includes two key components: the *environment* (including state transition and reward model), and the *agent*. Three elements (the state s, the action a, and the reward r) are exchanged in the interaction between the environment and the agent. In the following we elaborate these three elements which are crucial to our proposed deep reinforcement learning model.

1) The state $\mathcal{S} = \{s_t, t = 0, 1, \ldots, T\} \in \mathbb{R}^2$ describes the position of the focal zone, where t denotes the time stamp. In the training, s_0 is initialized as $s_0 = [(K' - \bar{K})/2, (K' + \bar{K})/2]$. Since the focal zone is a shifting fragment on 1-D $\mathbf{x}'_i$, we design two parameters to define the state: $s_t = \{\text{start}^t_{idx}, \text{end}^t_{idx}\}$, where start^t_{idx} and end^t_{idx} separately denote the start index and the end index of the focal zone.[2]
2) The action $\mathcal{A} = \{a_t, t = 0, 1, \ldots, T\} \in \mathbb{R}^4$ describes which the agent could choose to act on the environment. In our case, we define four categories of actions for the focal zone (as described in the state transition part in Fig. 2): left shifting, right shifting, extend, and condense. Here, at time stamp t, the state transition only choose one action to implement following the agent's policy $\pi : s_{t+1} = \pi(s_t, a_t)$.
3) The reward $\mathcal{R} = \{r_t, t = 0, 1, \ldots, T\} \in \mathbb{R}$ is calculated by the reward model, which will be detailed later. The reward model $\Phi : r_t = \Phi(s_t)$ receives the current state and returns an evaluation as the reward.
4) We employ the dueling deep Q networks (DQNs) [21] as the optimization policy $\pi(s_t, a_t)$, which is enabled to learn the state-value function efficiently. Dueling DQN learns the Q value $V(s_t)$ and the advantage function $A(s_t, a_t)$ and combines them: $Q(s_t, a_t) \leftarrow V(s_t), A(s_t, a_t)$. The primary reason we employ a dueling DQN to optimize the focal zone is that it updates all

[2]For example, for a random $\mathbf{x}'_i = [3, 5, 8, 9, 2, 1, 6, 0]$, the state $\{\text{start}^t_{idx} = 2, \text{end}^t_{idx} = 5\}$ is sufficient to determine the focal zone as $[8, 9, 2, 1]$.

the four Q values at every step while other policy only updates one Q value at each step.

2) Reward Model: Next, we introduce the design of the reward model, which is one important contribution of this paper. The purpose of the reward model is to evaluate how the current state impacts our final target which refers to the classification performance in our case. Intuitively, the state which can lead to the better classification performance should have a higher reward: $r_t = \mathcal{F}(s_t)$. As a result, in the standard reinforcement learning framework, the original reward model regards the classification accuracy as the reward. $\mathcal{F}$ refers to the WAS-LSTM. Note, WAS-LSTM focuses on the spatial dependency between different dimensions at the same time-point while the normal LSTM focuses on the temporal dependency between a sequence of samples collected at different time-points. However, WAS-LSTM requires considerable training time, which will dramatically increase the optimization time of the whole algorithm. In this section, we propose an alternative method to calculate the reward: construct a new reward function $r_t = \mathcal{G}(s_t)$ which is positively related with $r_t = \mathcal{F}(s_t)$. Therefore, we can employ $\mathcal{G}$ to replace $\mathcal{F}$. Then, the task is changed to construct a suitable $\mathcal{G}$ which can evaluate the interdimension dependency in the current state s_t and feedback the corresponding reward r_t. We propose an alternative $\mathcal{G}$ composed by three components: the autoregressive model [22] to exploit the interdimension dependency in $\mathbf{x}_i'$, the Silhouette Score [23] to evaluate the similarity of the autoregressive coefficients, and the reward function based on the silhouette score.

The autoregressive model [22] receives the focal zone $\bar{\mathbf{x}}_i$ and specifies that how the last variable depends on its own previous values. Then, to evaluate how rich information is taken in the autoregressive coefficients, we employ silhouette score [24] ss_t to interpret the consistence of $\boldsymbol{\varphi}$. The silhouette score measures how similar an object is to its own cluster compared to other clusters and a high silhouette value indicates that the object is well matched to its own cluster and poorly matched to neighboring clusters. Specifically, in our case, the higher silhouette score means that $\boldsymbol{\varphi}$ can be better clustered and the focal zone $\bar{\mathbf{x}}_i$ is be easier classified. At last, based on the $ss_t \in [-1, 1]$, we design a reward function

$$r_t = \frac{e^{ss_t+1}}{e^2 - 1} - \beta \frac{\bar{K}}{K'}.$$

The function contains two parts, the first part is a normalized exponential function with the exponent $ss_t + 1 \in [0, 1]$, which encourages the reinforcement learning algorithm to search the better s_t w that leads to a higher ss_t. The motivation of the exponential function is that: the reward growth rate is increasing with the silhouette score's increase.[3] The second part is a penalty factor for the focal zone length to keep the bar shorter and the β is the penalty coefficient.

In summary, the aim of focal zone optimization is to learn the optimal focal zone $\bar{\mathbf{x}}_i^*$ which can lead to the maximum reward. The optimization totally iterates $N = n_e * n_s$ times where n_e and n_s separately denote the number of episodes and steps [21]. ε-greedy method [25] is employed in the state transition.

[3]For example, for the same silhouette score increment 0.1, $ss_t : 0.9 \rightarrow 1.0$ can earn higher reward increment than $ss_t : 0.1 \rightarrow 0.2$.

D. Weighted Average Spatial LSTM Classifier

In this section, we propose WAS-LSTM classification for two purposes. The first attempt is to capture the cross-relationship among feature dimensions in the optimized focal zone $\bar{\mathbf{x}}_i^*$. The LSTM-based classifier is widely used for its excellent sequential information extraction ability which is approved in several research areas such as natural language processing [26]. Compared to other commonly employed spatial feature extraction methods, such as CNNs, LSTM less dependent on the hyper-parameters setting. However, the traditional LSTM focuses on the temporal dependency among a sequence of samples. Technically, the input data of traditional LSTM is 3-D tensor shaped as $[n_b, n_t, \bar{K}]$ where n_b and n_t denote the batch size and the number of temporal samples, separately.

In this paper, we transpose the input data as $[n_b, n_t, \bar{K}] \rightarrow [n_b, \bar{K}, n_t]$ following the equation $(A^T)_{ijk} = A_{ikj}$, in which form, each sample has shape $[\bar{K}, n_t]$ and the WAS-LSTM pays attention to each sample column and explores the latent dependencies between the various elements in the same column. WAS-LSTM aims to capture the dependency among various dimensions at one temporal point, therefore, we set $n_t = 1$.

The second advantage of WAS-LSTM is that it could stabilize the performance of LSTM via moving average method. In LSTM, each cell's output contains the information before it, however, the neural network's convergence and stability are fluctuated over different times of training. To enhance the convergence and stability, we calculate the LSTM outputs $\mathbf{O}_i$ by averaging the weighted past two outputs instead of only the final one (Fig. 2)

$$\mathbf{O}_i = w_1 \mathbf{O}_{i(\bar{K}-1)} + w_2 \mathbf{O}_{i\bar{K}}$$

where w_1 and w_2 are the corresponding weights which can adjust the importance proportion of $\mathbf{O}_{i(\bar{K}-1)}$ and $\mathbf{O}_{i\bar{K}}$. The weights can be automatically learned by the neural network [27] or be manually set. In this paper, we simply manually set $w_1 = w_2 = 0.5$ in order to save computing resources. The predicted label is calculated by $y_i' = \mathcal{L}(\bar{\mathbf{x}}_i^*)$ where $\mathcal{L}$ denotes the LSTM algorithm. ℓ_2-norm (with parameter λ) is adopted as regularization to prevent overfitting. The sigmoid activation function is used on hidden layers. The loss function is cross-entropy and is optimized by the AdamOptimizer algorithm.

III. Experiments

In this section, we design local real-world experiments to evaluate the efficiency and effectiveness of the proposed framework. First, the experimental setting is reported. Then, we compare our model with competitive state-of-the-art baselines and evaluate the performance in detail. Finally, we investigate the impact of crucial factors such as the framework latency and the reward model.

A. Experimental Setting

We conduct the EEG collection by using a portable and easy-to-use commercialized Emotiv Epoc+ headset. The

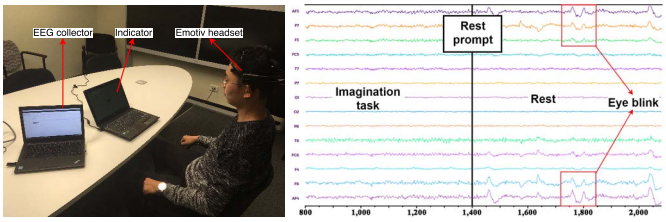

(a) (b)

Fig. 3. EEG data collection: (a) collection scenario and (b) gathered EEG signal.

TABLE I
IMAGERY ACTION, LABEL, AND CORRESPONDING COMMANDS IN CASE STUDIES

Imagery Action	Label	Typing Commands	Robot Commands
Upward	0	Up	Forward
Downward	1	Cancel	Turn Left
Leftward	2	Left	Grasp
Rightward	3	Right	Loose
Middle Cycle	4	Nothing	Nothing
Eye-closed	5	Confirm	Stop/Start

headset contains 14 channels and the sampling rate is 128 Hz. The local dataset can be accessed from this link.[4] This experiment is carried out using seven subjects (four males and three females) aged from 23 to 26. During the experiment, the subject wearing the *Emotiv Epoc+*[5] EEG collection headset, faces the computer screen and focuses on the corresponding *hint* which appears on the screen [shown in Fig. 3(a)]. EEG signals are recorded when the subject is imaging certain actions (without any physical action). The certain actions contains: upward arrow, downward arrow, leftward arrow, rightward arrow, and a cycle. Beyond that, the EEG signals that the subject stays relaxation with eye closed are also recorded. In total, there are six categories of EEG signals. The imagery action associated with brain activities and the corresponding labels used in this paper are listed in Table I. In summary, this experiment contains 241 920 samples with 34 560 samples for each subject. For each participant, the dataset is divided into a training set and a testing set. The training set contains 31 104 samples and the testing set contains 3456 samples. The classification results are evaluated by a number of metrics, including accuracy, precision, recall, F1-score, confusion matrix, receiver operating characteristic (ROC) curve, and area under curve (AUC) score.

B. Overall Comparison and Analysis

In the training stage, based on the tuning experience, the hyper-parameters setting are listed as follows. In the selective attention learning: the order of autoregressive is 3; $\bar{K} = 128$, the dueling DQN has four layers and the node number in each layer are: 2 (input layer), 32 (FCL), 4 $(A(s_t, a_t)) + 1$ $(V(s_t))$, and 4 (output). The decay parameter $\gamma = 0.8$, $n_e = n_s = 50$, $N = 2,500$, $\epsilon = 0.2$, learning rate$= 0.01$, memory size $=$ 2000, length penalty coefficient $\beta = 0.1$, and the minimum length of focal zone is set as 10. In the DL classifier: the node number in the input layer equals to the number of feature dimensions, three hidden layers with 164 nodes, two layers of LSTM cells (164 cells), and one output layer (six nodes). The learning rate $= 0.001$, ℓ_2-norm coefficient $\lambda = 0.001$, forget bias $= 0.3$, batch size $= 9$, and iterate for 1000 iterations.

[4][Online]. Available: https://drive.google.com/open?id=0B9MuJb6Xx2PIM0otakxuVHpkWkk

[5][Online]. Available: https://www.emotiv.com/product/emotiv-epoc-14-channel-mobile-eeg/

TABLE II
OVERALL COMPARISON WITH THE STATE-OF-THE-ART BASELINES. DL DENOTES DEEP LEARNING

Baselines	Methods	Metrics			
		Acc	Pre	Rec	F1-score
Non-DL	SVM	0.2569	0.2737	0.2569	0.2577
	RF	0.8041	0.8071	0.8041	0.8048
	KNN	0.8539	0.8563	0.8539	0.8544
	AB	0.2506	0.2039	0.2506	0.1557
	LDA	0.2595	0.2761	0.2595	0.2618
DL	LSTM	0.2609	0.2447	0.2348	0.2354
	GRU	0.2521	0.271	0.2696	0.2701
	CNN	0.725	0.724	0.7237	0.7238
The state-of-the-art	[28]	0.8965	0.9011	0.8926	0.8968
	[29]	0.7894	0.7938	0.8013	0.7975
	[30]	0.8891	0.8932	0.8765	0.8848
	WAS-LSTM	0.9026	0.9125	0.9003	0.9064
	SAM+WAS-GRU	0.9135	0.9188	0.9395	0.9378
	Ours	**0.9363**	**0.9394**	**0.9398**	**0.9396**

To demonstrate the efficiency of our approach, we compare our model with several competitive state-of-the-art methods.

1) Hsu [28] extracts several potential features, including amplitude modulation, spectral power and asymmetry ratio, adaptive autoregressive model, and wavelet fuzzy approximate entropy, followed by an SVM classifier, to classify the binary motor imagery EEG signals.
2) Tabar and Halici [29] combine convolutional neural networks (CNNs) and stacked Autoencoder (SAE) to automatically classify EEG data.
3) Martis *et al.* [30] artificially extracted several nonlinear features on different EEG frequency bands (including delta, theta, lower alpha, upper alpha, lower beta, upper beta, and lower gamma) and forward to SVM with radial basis function kernel.

Table II shows the overall comparison between our approach with nDL baselines, DL baselines, and the state-of-the-art models. RF denotes random forest, AdaB denotes adaptive boosting, and LDA denotes linear discriminant analysis. In addition, the key parameters of the baselines are listed here: linear SVM ($C = 1$), RF ($n = 200$), and KNN ($k = 3$). In LSTM, $n_{\text{steps}} = 5$, another set is the same as the WAS-LSTM classifier, along with the gated recurrent unit (GRU). The CNN contains two stacked convolutional layers (both with stride [1, 1], patch [2, 2], zero-padding, and the depth are four and eight, separately), one pooling layer (stride [1, 2], zero-padding) and one fully connected layer (164 nodes). Relu activation function is employed in the CNN.

The observations in Table II show that our approach outperforms all the baselines by achieving the highest accuracy of 0.9363 on the six-class classification. In addition, our model (SAM + WAS-LSTM) performs better than the solo WAS-LSTM, which demonstrates that the SAM has a positive contribution to the classification. The confusion matrix,

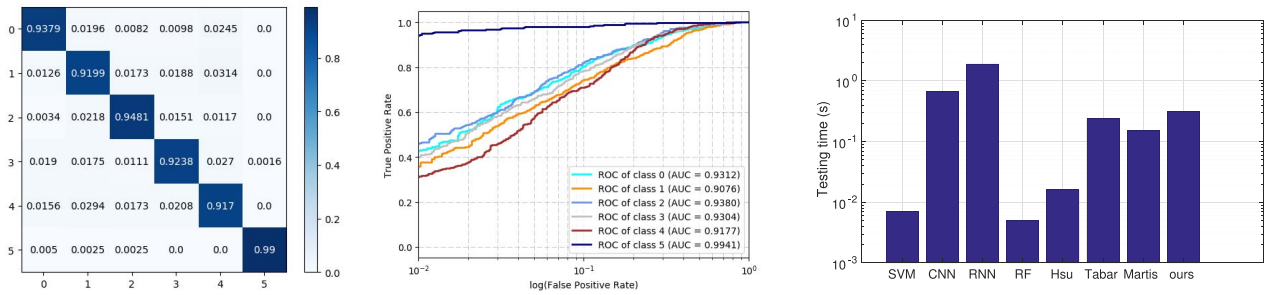

Fig. 4. Recognition results. (a) Confusion matrix. (b) ROC curves with AUC scores. (c) Latency.

ROC curves, and AUC scores of the proposed framework are reported in Fig. 4. We can observe that the last class, representing the eye-closed state, obtains the best performance compared to other five classes. This demonstrates that the eye-closed state is the easiest to be recognized, which is reasonable while all the other classes are in eye-open state and are easier to be interrupted by the environmental factors. Moreover, through the results comparison of SAM+WASGRU and our model (SAM+WASLSTM) (Table II), we can observe that the latter achieves higher performance which indicates ($0.9363 > 0.9135$) the LSTM slightly outperforms GRU in our scenarios. The reason can be inferred is that LSTM can remember longer sequences than GRU.

C. Impact of Key Factor

1) Latency: To design effective and real-world cognitive interactive applications, both the accuracy and latency of intent recognition are equally important. Subsequently, we compare the latency of the proposed framework with several typical state-of-the-art algorithms and the results are presented in Fig. 4(c). It is observed that our approach has competitive latency compared with other methods. The overall latency is less than 1 s. The DL-based techniques in this paper do not explicitly lead to extra latency.

2) Reward Model: Furthermore, we conduct extensive experiments to demonstrate the efficiency of the proposed reward model $\mathcal{G}$. First, we measure a batch of data pairs of the reward (represents the reward of $\mathcal{G}$) and the WAS-LSTM classifier accuracy (represents the reward of $\mathcal{F}$). The relationship between the reward and the accuracy is shown in Fig. 5. The figure illustrates that the accuracy has an approximately linear relationship with the reward. The correlations coefficient is 0.8258 (with p-value as 0.0115), which shows that the accuracy and reward are highly positive related. As a result, we can estimate $\arg\max_{\bar{\mathbf{x}}^*} \mathcal{F}$ by $\arg\max_{\bar{\mathbf{x}}^*} \mathcal{G}$. Moreover, another experiment is carried out to measure the single step training time of two reward models $\mathcal{G}$ and $\mathcal{F}$. The training times are marked as T1 and T2, respectively. Fig. 6 qualitatively shows that T2 is much higher than T1 (eight states represent eight different focal zones). Quantitatively, the sum of T1 over eight states is 35237.41 s while the sum of T2 is 601.58 s. These results demonstrate that the proposed approach, designing a $\mathcal{G}$ to approximate and estimate the $\mathcal{F}$,

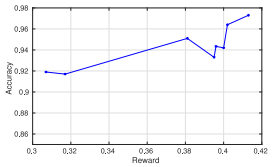

Fig. 5. Relationship between the classifier accuracy and the reward. The correlationship coefficient is 0.8258 while the p-value is 0.0115.

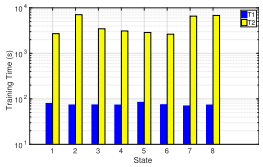

Fig. 6. Reward model training time in various states. T1 and T2 separately denote the training time in reward model $\mathcal{G}$ and $\mathcal{F}$.

saves $98.3\% = 1 - 601.58/35237.41$ training time in focal zone optimization.

IV. Case Study

Inspired by the high accuracy and low latency of our proposed framework for human intent recognition, we proceed to develop two real-world cognitive IoT prototypes: 1) a brain typing system and 2) mind-controlled assistive robot for the smart home.

A. Brain Typing System

Due to the high intent recognition accuracy, we develop an online brain typing system to convert user's thoughts to texts. The video demo clip can be found at the given link.[6] The brain typing system [Fig. 7(a)] consists of two components: the *pretrained deep learning model* and the *online BCI system*. The pretrained DL model, which is trained offline, aims to accurately recognize the user's typing intent in real time. The online system contains five components: 1) the EEG headset; 2) the client 1 (data collector); 3) the server; 4) the client 2 (typing command receiver); and 5) the typing interface. The user wears the Emotiv EPOC+ headset which collects EEG signals and sends the data to client 1 through a Bluetooth

[6][Online]. Available: https://youtu.be/Dc0StUPq61k

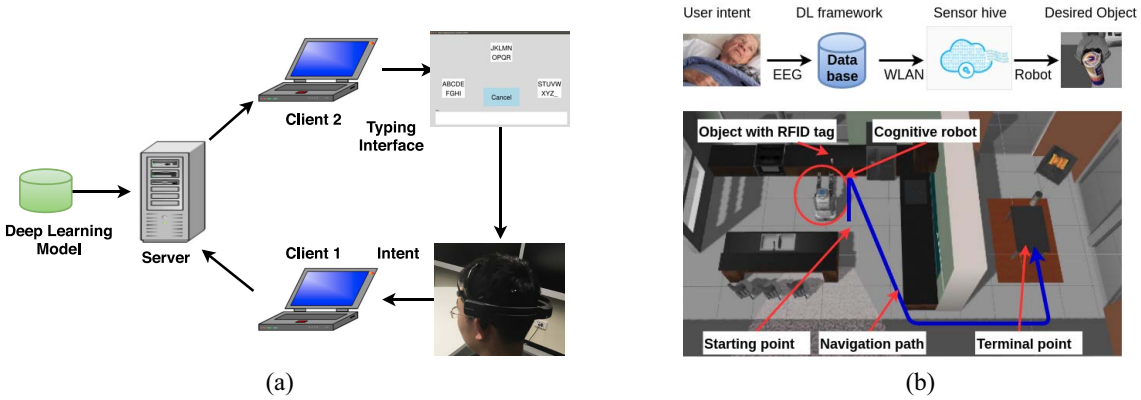

Fig. 7. Human-thing cognitive applications. (a) Brain typing system. (b) Cognitive robot in IoT scenario.

connection. The raw EEG signals are transported to the server through a TCP connection.

Specifically, the typing interface [up right corner in Fig. 7(a)] can be divided into three levels: 1) the initial interface; 2) the subinterface; and 3) the bottom interface. All the interfaces have similar structure: three *character blocks* (separately distributed in left, up, and down directions), a *display block*, and a *cancel button*. The display block shows the typed output and the cancel button is used to cancel the last operation. The typing system in total includes $27 = 3 * 9$ characters (26 English alphabets and the space bar) and all of them are separated into three character blocks (each block contains nine characters) in the initial interface. Overall, there are three alternative selections and each selection will lead to a specific subinterface which contains nine characters. Again, the $9 = 3 * 3$ characters are divided into three character blocks and each of them is connected to a bottom interface. In the bottom interface, each block represents only one character.

In the brain typing system, there are five commands to control the interface: "left," "up," "right," "cancel," and "confirm." Each command corresponds to a specific motor imagery EEG category (as shown in Table I). Since the user can hardly concentrate for a long time (usually, less than 10 s), the brain activity may represent none of the valid commands sometimes. Nevertheless, the proposed DL framework cannot distinguish the invalid brain activity, we leave one specific brain category to represent the invalid signal. If the individual's brain signal is not in any of the five valid categories, it is classified as the invalid category and the brain typing system will do nothing under this situation.[7] Moreover, based on the experiments results in Section III-B, the eye-closed state has the highest precision and accuracy, therefore, we select this state as the confirmation command for the reason that "confirmation" is the most crucial command in typing system. To type every single character, the interface is supposed to accept six commands. Consider typing the letter "I" as an example. The sequence of commands to be entered is as follows: left (choose the left block with characters $A \sim I$), confirm, right (choose the right block with characters $G \sim I$), confirm, right (choose the right block with characters I), confirm.

[7]Similarly, in the cognitive robot case, the robot will remain the previous state under the invalid command.

In our practical deployment, the sampling rate of Emotiv EPOC+ headset is set as 128 Hz, which means the server can receive 128 EEG recordings each second. Since the brainwave signal varies rapidly and is very easy to be affected by noises, the EEG data stream is sent to server *every half second*, which means that the server receives 64 EEG samples each time. The 64 EEG samples are classified by the DL framework and generate 64 categories of intents. we calculate the mode of 64 intents and regard the mode as the final intent decision. Furthermore, to achieve steadiness and reliability, the server sends the command to client 2 only if *three consecutive decisions remain consistent*. After the command is sent, the command list will be reset and the system will wait until the next three consistent decisions are made.

B. Cognitive Robot

Another important application for BCI-inspired IoT is extending the orientation of smart homes by integrating the subject's intent and the real-world IoT objects to effectively control things of interest.

To demonstrate the feasibility of the proposed framework, we report the second use case as implementing cognitive interactivity in an IoT-based smart home system. The IoT-based smart home is equipped with sensors, wherein IR sensors, ambient sound, heat, as well as contact sensors are mounted on furniture and used in the home environment in a nonintrusive manner. In our case, within the smart home environment which is perceived by the embedded sensor-networks, a simulated robot is cognitively navigated to perform a routine task. In the specific scenario, the robot, learns user's intent from EEG recordings via the proposed framework, to take the IoT object (e.g., a can of beverage) from a table in the kitchen and put it in a table in the living room. The desired object is aggregate with RFID tag which helps to identify the location. The IoT scenario is depicted in Fig. 7(b) and the demo can be found at here.[8] The user's intent is carried in the EEG recordings which are forwarded to the DL-based framework for interpretation. The recognized intent is send to sensor hive through WLAN to navigate the robot to get the desired object. Starting from the table near the kitchen, the PR2 robot receives action commands (as shown in Table I) and walks forward

[8][Online]. Available: https://youtu.be/VZYX1095Vkc

until the specific position with the auxiliary of RFID tag. Then, the robot grasps the object, turns back and walks along the path to the table in living room and unlooses hands to put the beverage on the table. The simulation result shows that the robot can 100% precisely grasp and unloose object according to the path planned in the subject's mind. The simulation platform is in Gazebo toolbox and the robot controlling program is powered by robot operating system. This case randomly selects some EEG raw data from Subject 1 dataset as simulation inputs.

V. Discussion

Here, we present several open challenges.

1) The experiment only contains seven subjects limited by the practical conditions, a larger and more diverse dataset is necessary to illustrate the effects of the proposed model.
2) The SAM component with focal zone is designed to automatically explore the latent dimension sequence of the input EEG data, nevertheless, the employment of SAM increases the training time resulted from more iterations of the LSTM cell.
3) Most importantly, the RS stage shuffles the order and replicate the number of input dimensions to discover the optimal order in order to the best performance, but the optimal order can not be guaranteed to appear after the RS, thus try more times if the classification result is unsatisfactory.
4) The WAS-LSTM exploits the spatial information among EEG channels, thus a number of channels are required to provide enough information.

VI. Conclusion

We propose a unified DL framework to bridge BCI and IoT in order to enable cognitive interactivity. We propose WAS-LSTM to extract interdimension dependency among the input signal of the human brain activities which are selected by the SAM. We conduct real-world experiments to evaluate the proposed framework and the results demonstrate that our model outperforms the state-of-the-art baselines. Furthermore, our experience in developing two case studies, namely the brain typing system and the cognitive robot, are reported in this paper. These case studies validate the feasibility of the proposed framework.

References

[1] L. Yao, Q. Z. Sheng, and S. Dustdar, "Web-based management of the Internet of Things," *IEEE Internet Comput.*, vol. 19, no. 4, pp. 60–67, Jul./Aug. 2015.

[2] A. Vallabhaneni, T. Wang, and B. He, "Brain–computer interface," in *Neural Engineering*. Boston, MA, USA: Springer, 2005, pp. 85–121.

[3] A. Teles *et al.*, "Using brain–computer interface and Internet of Things to improve healthcare for wheelchair users," in *Proc. 11th Int. Conf. Mobile Ubiquitous Comput. Syst. Services Technol. (UBICOMM)*, 2017, pp. 92–94.

[4] B. Jagadish, M. P. R. S. Kiran, and P. Rajalakshmi, "A novel system architecture for brain controlled IoT enabled environments," in *Proc. IEEE 19th Int. Conf. E-Health Netw. Appl. Services (Healthcom)*, 2017, pp. 1–5.

[5] X. Zhang *et al.*, "Converting your thoughts to texts: Enabling brain typing via deep feature learning of EEG signals," in *Proc. PerCom*, 2018, pp. 1–10.

[6] B. Nguyen, D. Nguyen, W. Ma, and D. Tran, "Investigating the possibility of applying EEG lossy compression to EEG-based user authentication," in *Proc. IEEE IJCNN*, 2017, pp. 79–85.

[7] T. Nakamura, V. Goverdovsky, and D. P. Mandic, "In-ear EEG biometrics for feasible and readily collectable real-world person authentication," *IEEE Trans. Inf. Forensics Security*, vol. 13, no. 3, pp. 648–661, Mar. 2018.

[8] M. A. Rahman and M. Ahmad, "Evaluating the connectivity of motor area with prefrontal cortex by fNIR spectroscopy," in *Proc. IEEE ECCE*, 2017, pp. 296–300.

[9] M. Iijima and N. Nishitani, "Cortical dynamics during simple calculation processes: A magnetoencephalography study," *Clin. Neurophysiol. Pract.*, vol. 2, pp. 54–61, Dec. 2016. [Online]. Available: https://www.sciencedirect.com/science/article/pii/S2467981X1630021X

[10] M. A. Rahman and M. Ahmad, "A straight forward signal processing scheme to improve effect size of fNIR signals," in *Proc. IEEE ICIEV*, 2016, pp. 439–444.

[11] E. Haselsteiner and G. Pfurtscheller, "Using time-dependent neural networks for EEG classification," *IEEE Trans. Rehabil. Eng.*, vol. 8, no. 4, pp. 457–463, Dec. 2000.

[12] Y. LeCun, Y. Bengio, and G. Hinton, "Deep learning," *Nature*, vol. 521, no. 7553, p. 436, 2015.

[13] M. Angelidou, "Smart city planning and development shortcomings," *TeMA J. Land Use Mobility Environ.*, vol. 10, no. 1, pp. 77–94, 2017.

[14] K. Dhariwal and A. Mehta, "Architecture and plan of smart hospital based on Internet of Things (IoT)," *Int. Res. J. Eng. Technol.*, vol. 4, no. 4, pp. 1976–1980, 2017.

[15] X. Zhang *et al.*, "Multi-modality sensor data classification with selective attention," in *Proc. IJCAI*, 2018, pp. 3111–3117.

[16] A. R. Al-Ali, I. A. Zualkernan, M. Rashid, R. Gupta, and M. Alikarar, "A smart home energy management system using IoT and big data analytics approach," *IEEE Trans. Consum. Electron.*, vol. 63, no. 4, pp. 426–434, Nov. 2017.

[17] L. Yao *et al.*, "WITS: An IoT-endowed computational framework for activity recognition in personalized smart homes," *Computing*, vol. 100, no. 4, pp. 369–385, 2018.

[18] X. Zhang, L. Yao, C. Huang, Q. Z. Sheng, and X. Wang, "Intent recognition in smart living through deep recurrent neural networks," in *Proc. Int. Conf. Neural Inf. Process.*, 2017, pp. 748–758.

[19] P. Cavanagh *et al.*, "Attention-based motion perception," *Science*, vol. 257, no. 5076, pp. 1563–1565, 1992.

[20] V. Mnih *et al.*, "Human-level control through deep reinforcement learning," *Nature*, vol. 518, no. 7540, pp. 529–533, 2015.

[21] Z. Wang *et al.*, "Dueling network architectures for deep reinforcement learning," in *Proc. 33rd Int. Conf. Mach. Learn.*, vol. 48, Jun. 2016, pp. 1995–2003.

[22] H. Akaike, "Fitting autoregressive models for prediction," *Ann. Inst. Stat. Math.*, vol. 21, no. 1, pp. 243–247, 1969.

[23] A. Laurentini, "The visual hull concept for silhouette-based image understanding," *IEEE Trans. Pattern Anal. Mach. Intell.*, vol. 16, no. 2, pp. 150–162, Feb. 1994.

[24] L. Lovmar, A. Ahlford, M. Jonsson, and A.-C. Syvänen, "Silhouette scores for assessment of SNP genotype clusters," *BMC Genomics*, vol. 6, no. 1, p. 35, 2005.

[25] M. Tokic, "Adaptive ε-greedy exploration in reinforcement learning based on value differences," in *Proc. Annu. Conf. Artif. Intell.*, 2010, pp. 203–210.

[26] F. A. Gers and E. Schmidhuber, "LSTM recurrent networks learn simple context-free and context-sensitive languages," *IEEE Trans. Neural Netw.*, vol. 12, no. 6, pp. 1333–1340, Nov. 2001.

[27] X. Zhang *et al.*, "MindID: Person identification from brain waves through attention-based recurrent neural network," in *Proc. ACM Conf. Pervasive Ubiquitous Comput. (UbiComp)*, 2018, Art. no. 149.

[28] W.-Y. Hsu, "Assembling a multi-feature EEG classifier for left–right motor imagery data using wavelet-based fuzzy approximate entropy for improved accuracy," *Int. J. Neural Syst.*, vol. 25, no. 8, 2015, Art. no. 1550037.

[29] Y. R. Tabar and U. Halici, "A novel deep learning approach for classification of EEG motor imagery signals," *J. Neural Eng.*, vol. 14, no. 1, 2016, Art. no. 016003.

[30] R. J. Martis *et al.*, "Epileptic EEG classification using nonlinear parameters on different frequency bands," *J. Mech. Med. Biol.*, vol. 15, no. 3, 2015, Art. no. 1550040.

Xiang Zhang (GS'17) received the master's degree from the Harbin Institute of Technology, Harbin, China, in 2016. He is currently pursuing the Ph.D. degree at the School of Computer Science and Engineering, University of New South Wales, Kensington, NSW, Australia.

His current research interests include deep learning, brain–computer interface, Internet of Things, and human activity recognition.

Lina Yao (M'14) received the Ph.D. degree in computer science from the University of Adelaide, Adelaide, SA, Australia.

She is currently a Lecturer with the School of Computer Science and Engineering, University of New South Wales, Kensington, NSW, Australia. Her current research interests include machine learning and data mining with applications to the Internet of Things, brain–computer interface, information filtering and recommending, and human activity recognition.

Dr. Yao is a member of the ACM.

Shuai Zhang (S'17) received the bachelor's degree from the School of Information Management, Nanjing University, Nanjing, China. He is currently pursuing the Ph.D. degree at the School of Computer Science and Engineering, University of New South Wales, Kensington, NSW, Australia, and Data61, CSIRO, Canberra, ACT, Australia.

His current research interests include recommender systems, deep learning, and Internet of Things.

Mr. Zhang is a member of the ACM.

Salil Kanhere (S'00–M'03–SM'11) received the Ph.D. degree from Drexel University, Philadelphia, PA, USA.

He is an Associate Professor with the School of Computer Science and Engineering, University of New South Wales, Kensington, NSW, Australia. He has authored or co-authored 170 peer-reviewed papers and delivered over 20 tutorials and keynote talks. His current research interests include the Internet of Things, pervasive computing, crowd sourcing, sensor networks, and security.

Dr. Kanhere was a recipient of the Humboldt Research Fellowship. He is a member of the ACM.

Michael Sheng (M'02) received the Ph.D. degree in computer science from the University of New South Wales (UNSW), Kensington, NSW, Australia.

He was a Post-Doctoral Research Scientist with the CSIRO ICT Centre, Canberra, ACT, Australia. He spent ten years with the School of Computer Science, University of Adelaide, Adelaide, SA, Australia. He is a Full Professor and the Head of the Department of Computing, Macquarie University, Sydney, NSW. From 1999 to 2001, he was also a Visiting Research Fellow with UNSW.

Yunhao Liu (M'04–SM'06–F'15) received the B.S. degree from the Automation Department, Tsinghua University, Beijing, China, the M.A. degree from Beijing Foreign Studies University, Beijing, and the M.S. and Ph.D. degrees in computer science and engineering from Michigan State University, East Lansing, MI, USA.

He is currently an MSU Foundation Professor and the Chairperson with the Department of Computer Science and Engineering, Michigan State University. He holds the Chang Jiang Chair Professorship (No Pay Leave) with Tsinghua University.